AGU PUBLICATIONS

JGR

Journal of Geophysical Research: Oceans

RESEARCH ARTICLE

10.1002/2015JC011435

Global characteristics of coherent vortices from surface drifter trajectories

Rick Lumpkin[1]

[1]NOAA/Atlantic Oceanographic and Meteorological Laboratory, Miami, Florida, USA

Key Points:
- Over 15,000 looping trajectory segments are identified automatically in drifter data
- Characteristics of the vortices advecting looping drifters are examined worldwide
- Many properties are significantly different between loopers and nonloopers

Correspondence to:
R. Lumpkin,
Rick.Lumpkin@noaa.gov

Citation:
Lumpkin, R. (2016), Global characteristics of coherent vortices from surface drifter trajectories, *J. Geophys. Res. Oceans*, *121*, 1306–1321, doi:10.1002/2015JC011435.

Received 2 NOV 2015
Accepted 20 JAN 2016
Accepted article online 25 JAN 2016
Published online 14 FEB 2016

Abstract An algorithm is developed that can automatically identify loopers in Lagrangian trajectory data, i.e., looping trajectories that complete at least two orbits, in a significant update to Griffa et al. (2008). This algorithm is applied to the Global Drifter Program data set, and over 15,000 looping trajectory segments are identified worldwide. While two third of these segments are 14–39 days long, some persist for hundreds of days; the longest looper in the record persisted for 287 days. The paths taken by the vortices at the center of these looper trajectory segments can be calculated from these data. The Lagrangian integral time scale can also be estimated for the looper segments, and is generally very close to the orbital period—a value several times larger than the integral time scales characterizing nonloopers. Fundamental time-mean quantities such as total kinetic energy and velocity are shown to be significantly different between loopers and nonloopers. These results suggest that a careful approach to the data might require separately calculating means of the nonloopers and loopers, and only afterward combining the weighted results for an overall time-mean picture. While many of the loopers with large radii orbit vortices identified in altimeter-derived eddy census data, many with smaller radii do not match vortices resolved in altimetry. The data from this study are available at http://www.aoml.noaa.gov/phod/loopers/.

1. Introduction

Because coherent vortices can trap Lagrangian particles for extended periods of time [*Flierl*, 1981], floats and drifters provide an extremely valuable tool to observe the distribution of vortex characteristics. This was exploited by *Richardson* [1993] in the subtropical North Atlantic by identifying "loopers" in the trajectories of 230 SOFAR floats. Richardson defined a looper as follows [*Richardson*, 1993]:

> Each trajectory was visually examined for loops and cusps revealing the characteristic motion of particles in eddies – a rotational velocity around the eddy center, plus its translation . . . Once a looping float trajectory (looper) was identified, consisting of around two or more consecutive loops in the same direction, various summary statistics were calculated and used to estimate the characteristics of the eddies.

With the resulting 35.4 float years of looping trajectories (~15% of the overall data), Richardson was able to show the distribution of size, swirl speed, sense of rotation (cyclonic versus anticyclone), and translation of subsurface eddies, and was able to infer their life cycle from formation through propagation. He also noted that the eddy kinetic energy of loopers is much higher than that of nonloopers, highlighting the significant role of coherent eddies in setting the distribution of oceanic *EKE*.

Richardson's [1993] approach required subjective calls for complex trajectories that may have been the superposition of looping and nonlooping motions (or of simultaneous looping at different frequencies), and was not a practical solution for extremely large data sets. More recently, *Veneziani et al.* [2004] introduced a methodology to automatically identify loopers in float trajectories. In this approach, the spin Ω is calculated as:

$$\Omega = <u'dv' - v'du'> / (2\Delta t\, EKE) \quad (1)$$

where u', v' are the zonal and meridional components of eddy speed, du', dv' are changes in u', v' over time increment Δt, and *EKE* is the eddy kinetic energy $0.5(<u'>^2 + <v'>^2)$. The spin Ω couples the zonal and meridional velocities and can be related to the vorticity of the Eulerian fluid field if the particle is in solid-

body rotation [*Veneziani et al*., 2005]. For circular motion, $u' = a\ \sin(2\pi t/P)$, $v' = a\ \cos(2\pi t/P)$, one finds that $du' = u'(t + \Delta t/2) - u'(t - \Delta t/2)$ and $dv' = v'(t + \Delta t/2) - v'(t - \Delta t/2)$, By substituting these into (1), using the trigonometric identities $\sin(a \pm b) = \sin(a)\cos(b) \pm \cos(a)\sin(b)$, $\cos(a \pm b) = \cos(a)\cos(b) \mp \sin(a)\sin(b)$, and assuming that $\Delta t \ll P$, one can derive that $<u'\ dv' - v'\ du'> = -2\pi a^2\ \Delta t/P$ and $EKE = a^2/2$, and thus the period P and radius R of a looping trajectory is:

$$P = 2\pi/|\Omega|, R = \sqrt{2EKE}/|\Omega| \tag{2}$$

Veneziani et al. [2004] examined the distribution of Ω and determined that trajectories exceeding $|\Omega| > 0.1$ days^{-1} were sufficiently looping that they approximately met *Richardson*'s [1993] definition, although they noted that some trajectories have very large values of $|\Omega|$ for less than two completed loops.

While this manuscript focuses upon the characteristics of vortices determined from looping trajectories, it is important to note that looping motion may be associated with motion other than coherent vortices such as direct wind forcing or waves. In these cases, the spin is not necessarily related to the vorticity. Even for particles trapped in vortices, it should be noted that the orbital radii provide a minimum estimate of the vortex radii; nothing prevents the vortices from being larger than the radii of the orbits.

Griffa et al. [2008, hereafter GLV08] used the approach of *Veneziani et al*. [2004] to automatically determine loopers in the global surface drifter data set also used in this study. GLV08 defined eddy velocity u' as the difference between total velocity u and $<U>$, the mean speed from a monthly climatology of surface currents [*Lumpkin and Garraffo*, 2005]. They examined drifters only with drogues attached (a later reanalysis of drogue presence [*Lumpkin et al*., 2012] determined that a significant fraction of these drifters had lost their drogues), and discarded drifters which were not on continuous duty cycle, e.g., drifters transmitting one out of every 3 days. GLV08 divided the drifter trajectories into 20 day nonoverlapping segments and low passed the velocities at 1.5 times the local inertial period to remove inertial oscillations. They found that a threshold of $|\Omega| > 0.4$ days^{-1}, where Ω is the mean value of spin over the 20 day segment, approximately separated looper from nonlooper trajectory segments. GLV08 showed that the global distribution of spin was significantly non-Gaussian, skewed toward cyclonic values and with a kurtosis of 1.50 ± 0.39 indicating extreme values much more likely to occur than in a Gaussian distribution. They also showed that cyclonic spin dominated in the latitude bands 10°N/S–20°N/S, while anticyclonic spin dominated in the bands 30°N/S–40°N/S. The radii of looping trajectory segments were generally large where *EKE* is large, consistent with energetic rings associated with major ocean currents such as the Gulf Stream, Kuroshio, and Agulhas. Small radii were associated with high-latitude anticyclones, which GLV08 attributed to the Ekman response to subinertial wind forcing. Small radii were also associated with the 10°N/S–20°N/S cyclonic bands, attributed to submesoscale vortices associated with subtropical frontal instabilities.

In this study, loopers in the drifter data examined by GLV08 are reexamined using a new methodology that (1) does not require trajectories to be divided into fixed-length segments and (2) does not impose a minimum value of $|\Omega|$ in order to define a looper. The advantage of (1) is that many of the 20 day segments are only partially looping (i.e., looping begins or ends during the segment), and many loopers persist in looping for more than 20 days. The advantage of (2) is twofold: first, a meaningful comparison of the distribution of spin for loopers and nonloopers can be conducted. Second, the GLV08 cutoff of $|\Omega| > 0.4$ days^{-1} is equivalent to discarding all loopers with orbital period longer than 15.7 days; these can be retained with the methodology presented here.

Since the publication of GLV08, two studies have presented alternatives to automatically detect looping trajectories. *Dong et al*. [2011] presented a geometrical-based methodology that identifies trajectories which cross themselves in at least two closed loops, with a mean period larger than the inertial period but smaller than 90 days. However, as illustrated by *Dong et al*. [2011, Figure 5], the methodology identifies *any* closed trajectory segments as looping, regardless of how irregular the trajectory is during that segment, and additional filtering is necessary to identify vortices. The methodology presented here rejects noncircular/noncycloidal trajectories by requiring that spin Ω does not change sign during the looping.

Lilly and Olhede [2010] and *Lilly et al*. [2011] presented a powerful methodology that extracts values of the slowly varying amplitude, eccentricity, and orientation of an elliptical signal embedded within in a velocity time series. The elliptical motion can range from a perfect circle to purely back-and-forth linear displacement. The most significant differences between the methodology presented here and that of *Lilly and*

Olhede [2010, hereafter LO10] is that the methodology in this study provides an aggregate measure of rotation within a time series, combining effects from the full range of subinertial frequencies, while LO10 provides a local methodology intended to extract instantaneous values characterizing oscillatory motions from a time series (J. Lilly, personal communication, 2015). In addition, the methodology presented here explicitly places weight upon the persistence of looping. The methodology presented here is more simple and direct than LO10, and focuses on the nearly circular trajectories of drifters trapped in coherent vortices while rejecting wave-like orthogonal displacements that can be detected with LO10. In the case of strong looping motion with respect to the background flow, the two methods should produce similar results. In summary, the main strength of the LO10 methodology is its flexibility: it produces a time series of slowly varying parameters describing arbitrary oscillatory motion in a time series (Eulerian or Lagrangian), including classes of motion besides nearly circular looping. The main strengths of the methodology presented here are that it is specifically tuned to identify loopers as defined by *Richardson* [1993], i.e., the motion of Lagrangian particles caught in coherent vortices, and that it is relatively simple to implement.

2. Data

This study uses quality-controlled surface drifter data from the Global Drifter Program [*Lumpkin and Pazos*, 2007]. The data spanned the time period February 1979 through December 2014. Positions were interpolated via kriging to regular 6 h intervals [*Hansen and Poulain*, 1996]. Drogue presence was identified using the methodology described in *Lumpkin et al*. [2012]. Drifters with a duty cycle (on/off cycle, used in older drifters to save power) of half or less were removed, as in GLV08, as the often-used cycle of 1 day on and 2 days off could greatly distort higher-frequency looping trajectories [e.g., *Flament et al*., 2001].

Velocities every 6 h were obtained via 12 h centered differencing of the kriged positions. NCEP operational 6 h surface (0.995 sigma level) winds W were interpolated to the drifter locations, and a downwind slip of 7×10^{-4} W [*Niiler et al*., 1995] is removed. The resulting velocities were low passed with a two-point Butterworth filter with half-power cutoff at 1.5 times the local inertial period (IP), or 5 days if shorter than 1.5 IP, to remove tidal and near-inertial components of the flow. The resulting data set consisted of 15,602 drifter-years of data, collected by 16,407 unique drifters.

In a preliminary implementation of the methodology (and following both GLV08 and *Dong et al*. [2011]), the large-scale flow, calculated as described in *Lumpkin and Johnson* [2013], was interpolated to the drifter observations and removed in order to derive eddy fluctuations. However, as shown later, looping drifters can exhibit markedly different mean displacements than those of nonlooping drifters in the same region. Because nonlooping drifters dominate the data set, and thus the mean current climatology, looping trajectories in regions of strong mean currents were often heavily distorted with respect to their mean displacement. In some cases, this distortion was so severe that the methodology failed to identify them as loopers, while it was successful if the mean had not been removed. To avoid this, the total velocity, low passed as described above, was used for purposes of identifying loopers. This approach assumes that the total velocity measured by a drifter is dominated by the eddy fluctuating component rather than the time-mean velocity. For nonloopers, the time-mean component is significant in currents such as the Gulf Stream, Kuroshio, and Antarctic Circumpolar Current. However, it is in precisely these regions that the nonloopers and looper mean velocities differ most significantly, as shown later in this study. Including the time mean component in these regions does not result in false positive detection (nonloopers identified as loopers), while removing it does result in false negative detection (loopers failing to be identified).

3. Methodology: Automatic Looper Detection

As the methodology was developed, it was evaluated for performance using a small subset of the data with clearly identifiable periods of looping behavior (e.g., Figure 1). The methodology was designed so that it would automatically detect segments of drifter trajectories which exhibit sustained looping that had previously been identified manually. More rigorous quantified testing is described in section 3.1.

In order to identify periods of sustained looping, the spin Ω (equation (1)) is calculated and smoothed by a running 3 day median filter from the beginning to the end of each drifter's velocity time series. This smoothing was necessary to avoid spurious changes in the sign of Ω associated with position noise or brief

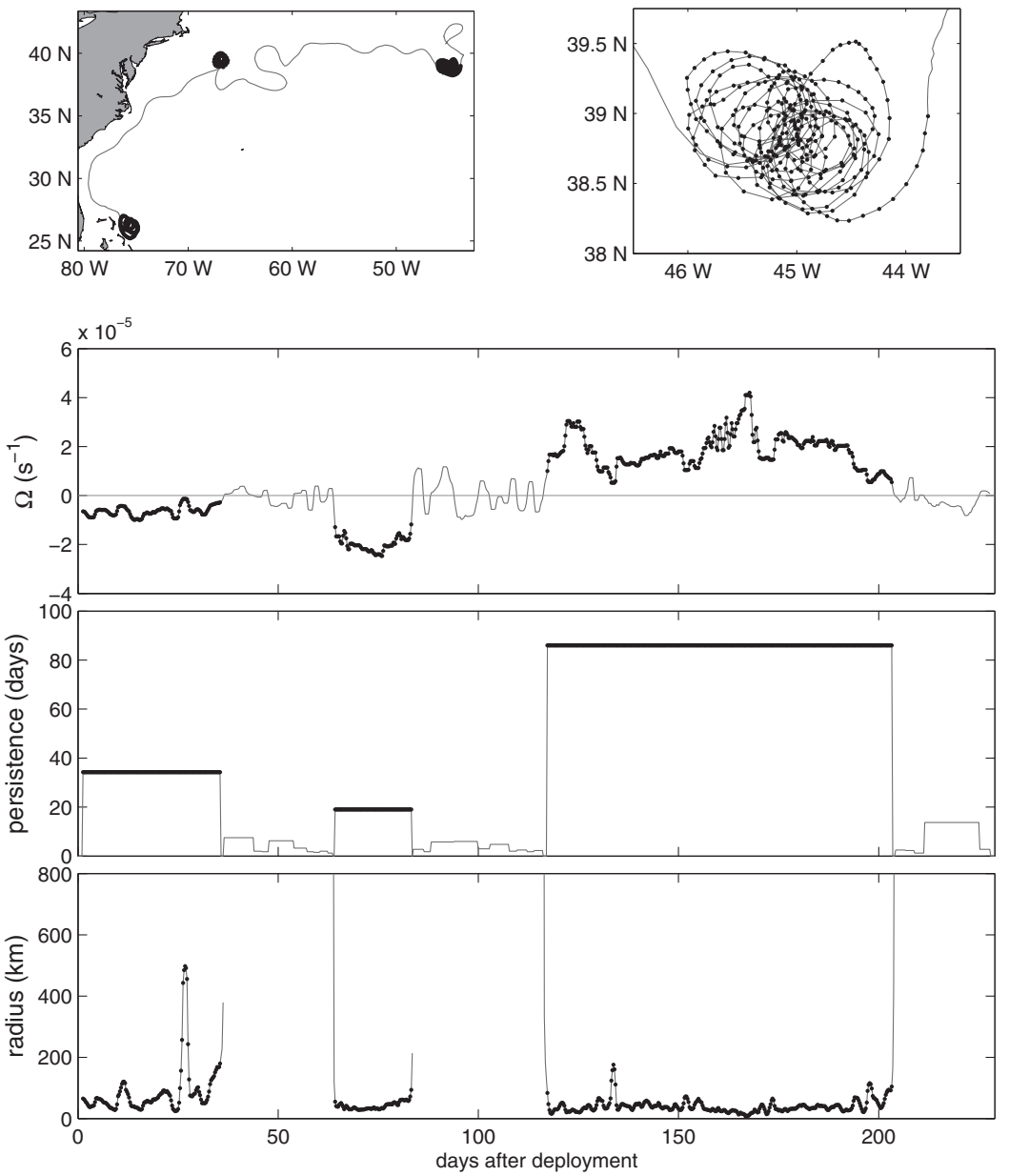

Figure 1. example of the methodology applied to drifter ID 47577, deployed east of the Bahamas. (top left) Total trajectory (grey), including segments automatically identified as looping (black dots). (top right) Close-up of final looping segment. (top middle) Spin Ω, median low passed at 3 days. (middle) Persistence. When persistence exceeds twice the theoretical period, the segment is flagged as looping in the first iteration. (bottom) Radius *R*. End points with *R* exceeding 3 times the median during looping are not identified as looping in the second iteration. In all plots, black dots indicate quarter-day values identified as looping.

variations from otherwise continuously looping behavior; the choice of 3 days is arbitrary, and was chosen to best match results from automatic detection with manual evaluation of continuous looping versus interrupted looping. Once the smoothed Ω is calculated, the trajectory is broken into segments delineated by zero crossings of Ω (see Figure 1 for an example). The duration of each segment of sustained positive or negative Ω, hereafter called the "persistence," is calculated. For each segment, the period *P* is calculated as $2\pi/|\Omega^*|$, where $|\Omega^*|$ is the absolute value of the median of Ω over the segment. This period is then compared to the persistence. If the persistence is at least twice *P*, i.e., at least two orbits were completed with either positive or negative Ω, then the segment is flagged as a looper.

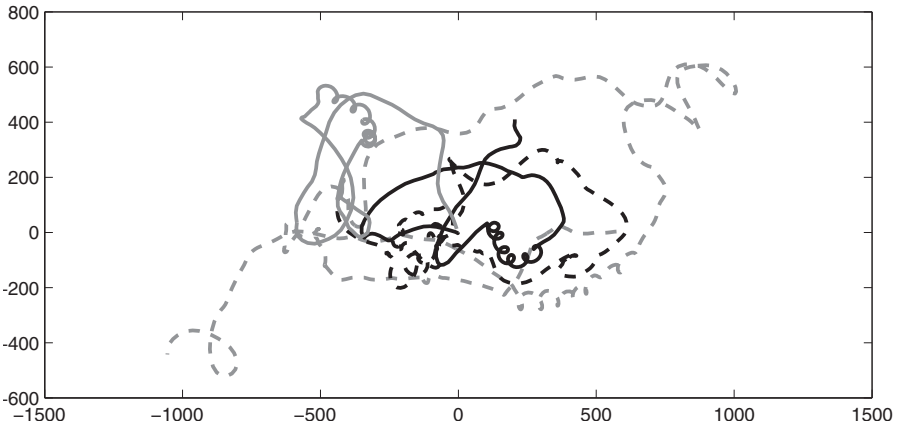

Figure 2. Two examples of 60 day synthetic drifter trajectories (x', y') (km) exhibiting loops of period 5 days for 30 days (solid black and grey) and two real trajectories from the Global Drifter Program data set with ∼5 day looping for ∼30 of the 60 days shown (dashed black and grey). The synthetic drifters have $N/A = 0.3$ (see text).

In a second iteration, points at the beginning and end of the looper segment are rejected as nonlooping where the radii R, calculated from (3), exceed 3 times the median value of R during the looping segment (Figure 1). This was done to reject points immediately preceding or following looping, when a trajectory has the same sign of Ω as during looping but still a nearly straight line (anomalously small Ω, large R compared to the clearly looping part of the segment). The choice of 3 times median R is subjective; larger values result in more frequent cases of "false positives," in which the trajectory before or after looping is erroneously flagged as looping, while smaller values result in looping segments flagged as nonlooping for large initial or final orbits. Note that this rejection was only done at the beginning or end of a segment identified as looping; larger values of R are permitted within the looping segment (e.g., Figure 1).

3.1. Evaluation of Methodology Using Synthetic Trajectories

The methodology was tested using thousands of synthetic drifter trajectories for which the orbital characteristics and other parameters could be exactly determined. The synthetic trajectories were each 60 days long and constructed to be nonlooping except on days 20–50 when they were looping. For the nonlooping days, the trajectories were described by a Matérn process of the form $E(f) = B^2/(f^2 + h^2)^\delta$ [*Sykulski et al.*, 2013], where $E(f)$ is the energy density spectrum of eddy velocity u' or v', f is frequency in cycles per day, and the coefficients were chosen so that the spectrum closely resembles the globally averaged mean spectrum of nonloopers (shown later in this manuscript): $B = 0.011$ m^2/s^2, $h = 0.1$ cpd, and $\delta = 1.6$. On days 20–50, the looping synthetic trajectories were determined by integrating $u' = A\,sin(2\pi t/P) + n$, $v' = A\,cos(2\pi t/P) + n$, where $A = 0.3$ m/s is the amplitude of the looping velocity, P is the period, and n is random noise of standard deviation N m/s with a spectral slope of -3. (Initially, the looper model was superimposed on the background Matérn process, rather than replacing it, during the looping segment of the synthetic trajectory. However, the resulting looping segment tended to be far more distorted than looping segments in real trajectories. In other words, a lower level of noise (or unrealistically large looping speeds) had to be imposed to accurately simulate observed looping behavior.) Examples of the synthetic trajectories (integrals of u' and v') are shown in Figure 2 for $P = 5$ days and $N = 0.09$ m/s, along with two real drifters that exhibited a similar duration of looping with a period near 5 days. Apart from the instantaneous transition to looping in the synthetic drifters (desirable so that looping versus nonlooping is clearly differentiated for methodology evaluation) and constant looping radius, the synthetic trajectories are indistinguishable from the real ones.

Figure 3 quantifies the success of the methodology for a range of noise N divided by looping amplitude A. The top plot indicates the ratio of the period identified by the method to the true period, with the period determined from Ω (black markers) and from the fit to the velocity autocorrelation function (grey markers), during the segment identified as a looper. The ratio is very close to unity for small N/A, and remains close to unity for the autocorrelation method. The period derived from Ω increases from the true value with increasing noise, because noise tends to decrease the numerator of (1) (which is sensitive to correlations) more quickly than it decreases the denominator. Later, it is shown that the median period derived from Ω is 1.3

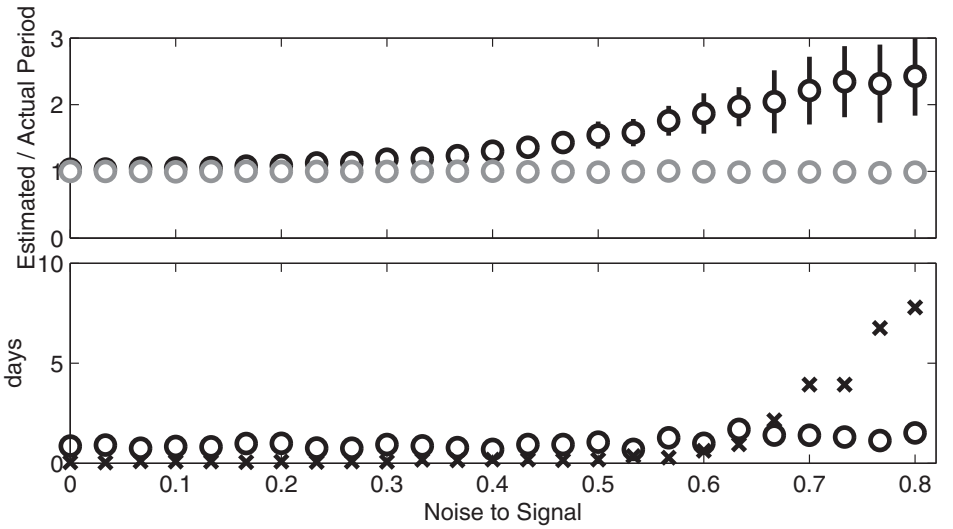

Figure 3. (top) Ratio of estimated period to actual period (vertical axis) for the synthetic drifters, with standard deviations, as a function of noise to signal *N/A* (horizontal axis). Black: period estimated from spin Ω. Grey: period estimated from fit to the velocity autocorrelation function. Error bars indicate standard errors, which do not reflect systematic errors at large *N/A*. (bottom) Number of days of the synthetic trajectory falsely flagged as looping (circles) and number falsely flagged as not looping (x) as a function of *N/A*. The synthetic drifters looped for 30 of the 60 days.

times larger than that derived from the autocorrelation for all loopers in the real drifter data, consistent with a mean value of $N/A \sim 0.3$ in Figure 3 (top). This result is not sensitive to the choice of period *P* for the simulated drifters as long as at least two loops are completed (and thus the trajectory is truly a looper).

Figure 3 (bottom) shows the number of drifter-days of synthetic data falsely flagged as looping (circles, "false positives") and the number of drifter-days falsely flagged as not looping (cross, "false negatives"). When the noise level is low, the method tends to slightly overestimate the persistence of looping by one half to 1 day, an overestimate 2–3%. As the noise increases past approximately $N = 0.65A$, the random motion overwhelms the looping behavior and the methodology increasingly fails to identify the entire looping segment. This result is sensitive to the choice of period *P* for the synthetic drifters, with fewer completed loops increasing the number of false negatives as a function of *N/A*. This limit is not seen as a weakness of the particular methodology presented here, as visual inspection of trajectories with large noise suggests that looping is difficult to assess manually as well.

3.2. Evaluation of Methodology Using Actual Trajectories

The methodology was evaluated by randomly selecting several hundred trajectories, plotting them (low passed to remove inertial oscillations and other superinertial looping) with segments of the trajectories identified as loopers highlighted, and evaluating this automatic detection against manual determination of looper segments [à la *Richardson*, 1993]. Each trajectory was evaluated both for possible false positives (automatic detection as a looper, but not passing manual visual inspection) and for false negatives (passing manual visual inspection as a looper, but not automatically detected). No false positives were identified during this evaluation process.

As noted earlier, a preliminary version of the detection algorithm was based upon eddy velocities derived by removing monthly mean currents from the total drifter velocity. During this manual evaluation, it was determined that numerous false negatives were identified in the Gulf Stream and Kuroshio regions. In these cases, a strong eastward velocity corresponding to the time-mean currents had been removed, but the loopers (in rings north or south of the instantaneous current) were propagating westward. As shown later, the mean speed of loopers is often radically different than the overall mean speed of all drifters. Removing the mean velocity from these trajectories resulted in grossly distorted trajectories, difficult to manually identify as cycloids, which failed to be detected as loopers by the algorithm. As a consequence, the time mean velocity was not removed in the final version of the algorithm.

4. Results

A total of 7.6% of the overall drifter data, representing 15,602 drifter-years of data, was automatically identified as loopers. For comparison, with the GLV08 cutoff of $|\Omega| > 0.4$ days^{-1}, 16.4% of the 20 day trajectory segments were identified as loopers. This suggests that "loopers" were often misidentified in GLV08 because of anomalously large values of mean spin that did not persist for at least two periods. The looping segments of the drifter trajectories identified in this study are shown in Figure 4, color coded by sign of vorticity. Some features of Figure 4 are well documented in the literature and shown, for example, in GLV08: the dominance of cyclonic loops to the south, and anticyclonic loops to the north, of the Gulf Stream and Kuroshio extensions; energetic anticyclones propagating west-southwestward from Tehuantepec, Mexico; both cyclones and anticyclones propagating westward from the Hawaiian and Canary islands; anticyclonic Agulhas rings and cyclonic eddies propagating into the South Atlantic from the Agulhas retroflection; anticyclonic North Brazil Current rings propagating west-northwestward from the North Brazil Current retroflection; the anticyclonic Great Whirl in the northwestern Indian Ocean. Anticyclonic cusps associated with Tropical Instability Waves (TIWs) are seen at near-equatorial latitudes, not resolved in GLV08 because the equatorial band was masked in that study. Other features of Figure 4 are less well known, such as the low-latitude band of submesoscale cyclones (particularly visible in the South Atlantic; GLV08); the extremely sharp meridional change in loop radius between the large TIWs and the small anticyclonic vortices immediately to their north in the tropical North Pacific.

Figure 5 shows global histograms of looper persistence, looper period, and looper radius for each looping trajectory segment (top) and histograms of spin, period and radius for all 6 h looper observations (bottom). The distinction between the top and bottom plots is that the top plots are values averaged over a looping trajectory segment, such that a 10 day looper and a 60 day looper are weighed equally in the histogram; the bottom plots weigh the latter more heavily by a factor of 6. The overlapping histograms of spin for loopers and nonloopers (Figure 5, bottom left) show that nonloopers can have large instantaneous values of spin while failing to meet the Richardson criterion for loopers, due for example to sharp bends in the trajectories, but that nonloopers clearly dominate low-spin values in the data. The outliers in the nonlooper distribution explain why GLV08 found a larger percentage of the data were loopers, because trajectory segments containing these outliers could be identified as loopers using the methodology of GLV08. The mean (median) persistence of all looping trajectories is 27.7 (23) days, with a mean (median) period of 8.3 (7.7) days and mean (median) radius of 26.7 (21.1) km. Two thirds of the loopers had persistence of 14–39 days, while one sixth were briefer and one sixth were longer. At the extreme tail of the persistence distribution, there were 44 trajectory segments that looped for longer than 150 days. The most persistent loopers were in two separate anticyclonic Agulhas rings (drifter IDs 9619845 and 52834, persistence 287 days and 260 days, respectively), in cyclonic rings south of the Gulf Stream (ID 55144, persistence 270 days) and Kuroshio (ID 94155, persistence 287 days) currents, and in a nearly stationary cyclonic vortex northeast of Kerguelen Island (ID 18749, persistence 252 days).

Figure 6 shows the median value of spin, persistence, period and radius for all 6 h observations flagged as looping. As found by GLV08, anticyclonic spin (yellow to red in top left plot) dominates at 30°N/S–40°N/S away from boundary currents while cyclonic spin dominates at ~20°N/S. Bands dominated by anticyclonic spin are also resolved at near-equatorial latitudes, associated with TIWs. GLV08 associated the higher-latitude anticyclonic spin bands with subinertial Ekman motion [e.g., *Elipot*, 2006]. The low-latitude cyclonic vortices are extremely small, as seen in the median radius plot (Figure 6, bottom right), and were related to submesoscale frontal vortices by GLV08. As shown by *Veneziani et al*. [2014], these vortices act to thicken barrier layers and produce a shallower mixed layer. Apart from these bands, looper radius generally decreases poleward, reflecting the distribution of the Eulerian length scale of eddies [*Stammer*, 1997], and away from regions of large *EKE*, following the distribution of Lagrangian length scales [*Lumpkin et al*., 2002]. The reader is reminded that these radii are a minimum estimate of vortex size, as nothing prevents a vortex from being larger than the orbital radius of a drifter trapped within it. Apart from a maximum associated with TIWs, the median period of looping (Figure 6, bottom left) does not vary spatially as dramatically as radius, as noted by GLV08.

Given the time-varying period and location of looping drifters, it is possible to estimate the paths taken by the vortices which had trapped the drifters. This can be done by a two-iteration process, after calculate the

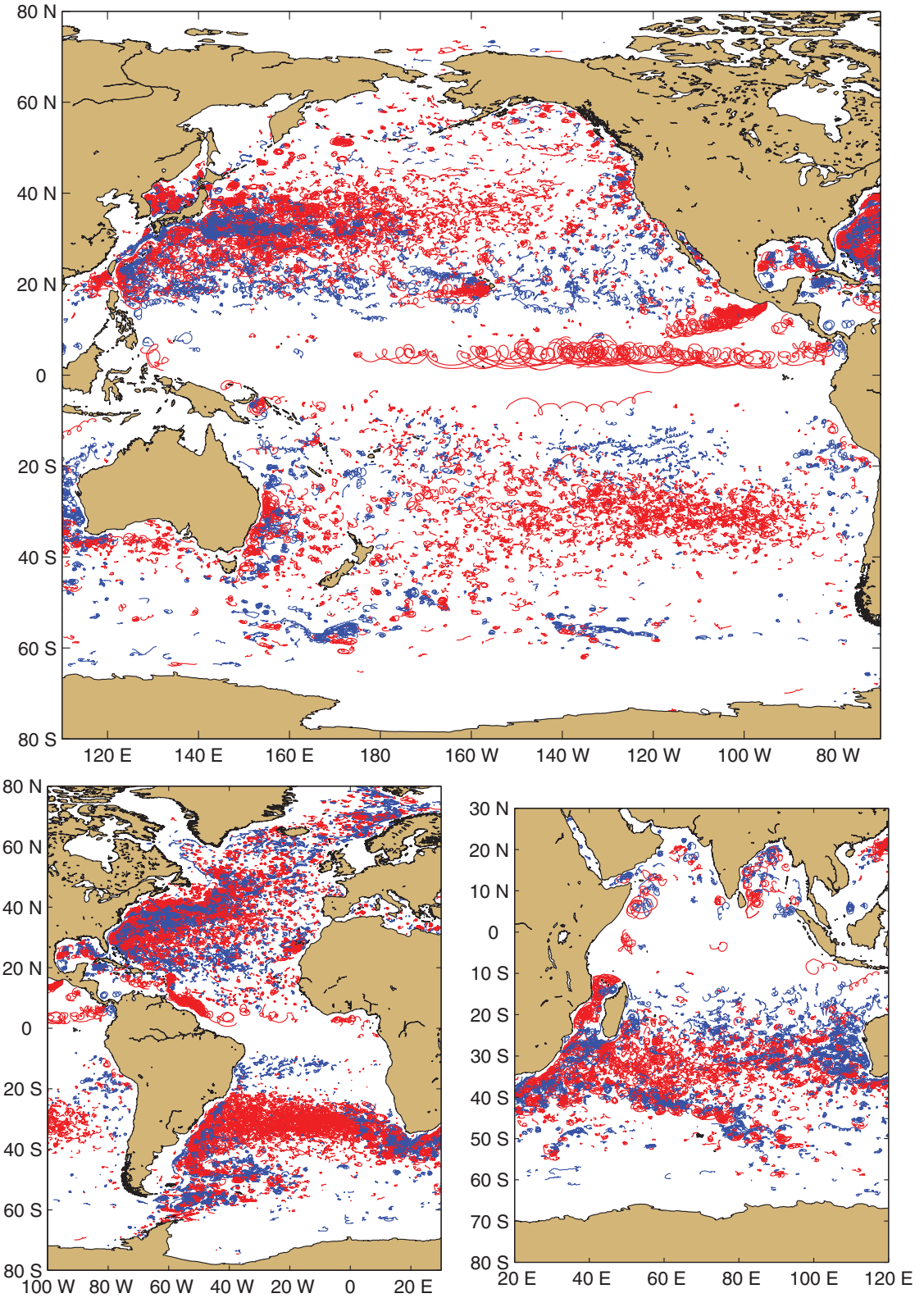

Figure 4. Trajectories of cyclonic (blue) and anticyclonic (red) loopers identified in the drifter data.

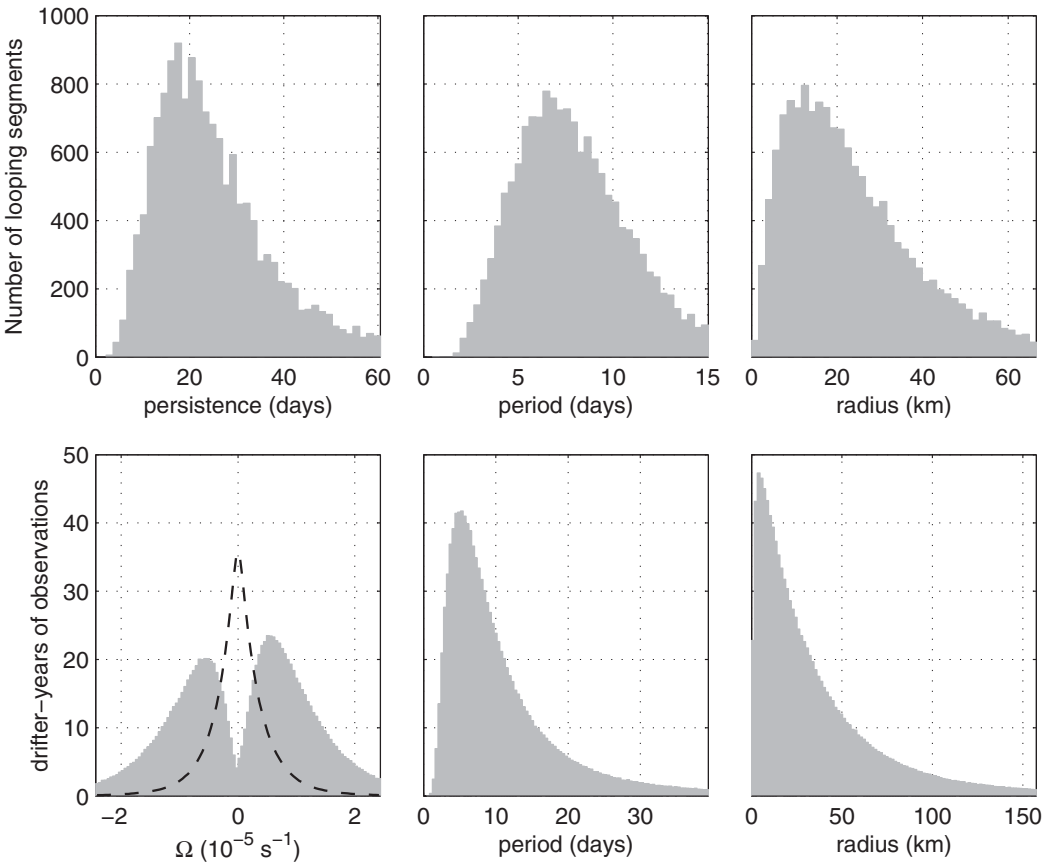

Figure 5. (top) Histograms of (left) persistence, (middle) period, and (right) radius of looping trajectory segments. (bottom) histograms of (left)spin, (middle) period, and (right) radius of all 6 h drifter observations flagged as a looper (gray). The histogram of spin for nonlooper observations (black, dashed line) is shown for reference in the bottom left plot, with the number of drifter-years divided by 25 so that it can be shown in the same scale. In all six looper histograms, 95% of the values are shown; the remaining 5% are in the tails of the distributions.

overall median period P_{med} of the looper trajectory segment (which, by definition, loops at least $2P_{med}$): (1) for every point i in the looper trajectory at time t_i, calculate the median period $P(t_i)$ in the window $t_i - P_{med}/2$ to $t_i + P_{med}/2$. (2) If points spanning this range exist, calculate the mean latitude and longitude in the window $t_i - P(t_i)/2$ to $t_i + P(t_i)/2$. This mean location over one orbit is the approximate center of the vortex at time t_i. Figure 7 (top) shows the propagation pathways of cyclonic (blue) and anticyclonic (red) eddies in the Hawaiian Island region derived using this approach applied to the looper trajectories, revealing the pathways of eddies generated in the lee of the islands [*Lumpkin and Flament*, 2001]. In a frame of reference moving with the automatically determined eddy center, the cycloidal trajectories of a looper becomes concentric circles (Figure 7, bottom left) and the eddy structure can be examined by plotting the (predominantly azimuthal) velocity versus distance from eddy center (Figure 7, bottom right). In the example shown in Figure 7, drifter 22938 was caught in the solid-body core of an anticyclonic eddy that slowly increased in orbital period from ~5 days in August 2003 to ~7 days in December 2003.

Figure 8 (top) shows the mean autocorrelation functions for zonal (R_{uu}) and meridional (R_{vv}) speeds and cross-correlation function R_{uv}, for looper and nonlooper trajectory segments in the subtropical North Atlantic region 18°N–32°N, 30°W–72.5°W (the same region used for Figure 1 of GLV08). The mean velocity autocorrelation function of nonlooper trajectory segments resembles a decaying exponential without significant negative lobes, while the mean of all loopers has a significant negative lobe between lags of 1.4–9.6 days. The cross-correlation function of nonloopers remains close to zero for all lags, while the mean of loopers shows the lagged correlation between zonal and meridional speed with peak correlations of 0.5–0.6 at a lag of 0.8–1 day. Mean orbital period over each looping trajectory segment can be estimated from the zero

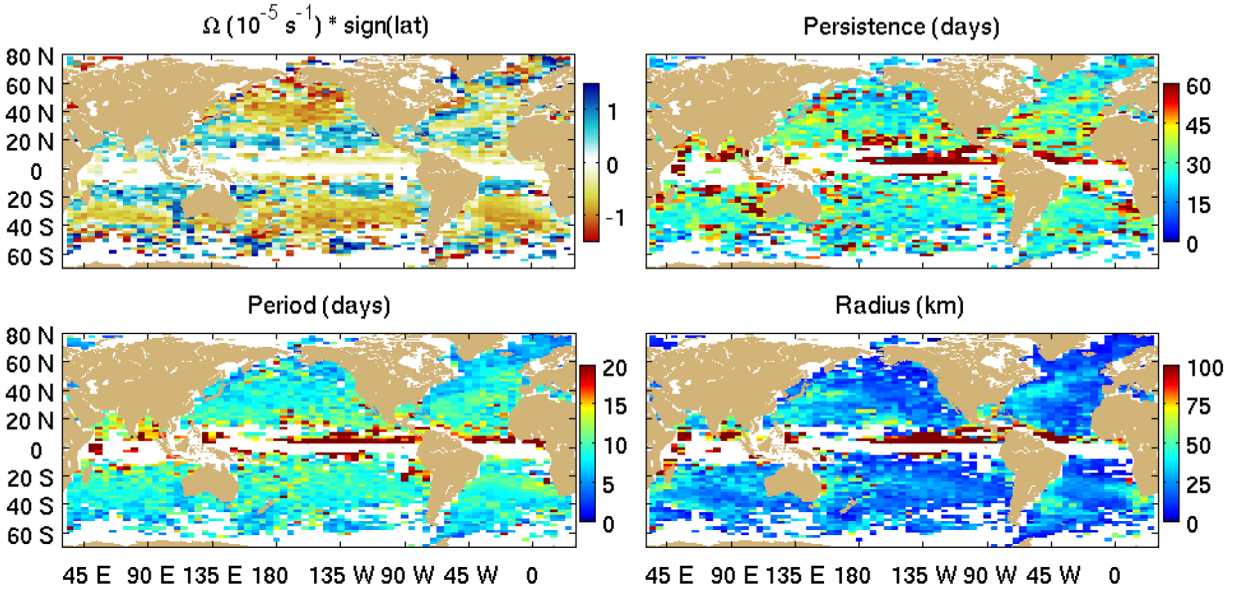

Figure 6. Median values of (top left)spin (multiplied by sign(latitude) so that anticyclonic is red, cyclonic is blue), (top right) persistence, (bottom left) period, and (bottom right) radius for all 6 h observations flagged as loopers. Values not shown if less than five drifter days are in a bin.

crossings of the autocorrelation function; the median value of $P = 2\pi/|\Omega|$ over each segment is on average 1.36 times larger than the autocorrelation-derived estimate, implying a signal-to-noise ratio of ~0.3 (see Figure 3). Loopers in the subtropical North Atlantic region have periods ranging from 1.4 to 28 days with a median of 6.6 days; if the lags for each individual looper auto-correlation and cross-correlation functions are first normalized by the period, then averaged, the result (Figure 8, bottom) shows strong oscillations to three periods lag, with an *e*-folding scale very close to one period. As noted by *Veneziani et al*. [2004], one can write the auto-correlation and cross-correlation functions for loopers as

$$R_{uu} = R_{vv} = \exp(-t/T_L) \cdot \cos(2\pi t/P), \quad R_{uv} = \exp(-t/T_L) \cdot \sin(2\pi t/P),$$

where T_L is the Lagrangian integral time scale. Thus, the Lagrangian time scale can be determined from the loopers by fitting a decaying exponential to the maxima (and −1 times minima) of each segment's autocorrelation and cross-correlation functions, and is close to the looping period. Globally, this calculation yields a spatial distribution of integral time scales (not shown) closely resembling the distribution of looper period (Figure 6, bottom left). However, these values are generally much higher than integral time scales reported in the literature [e.g., *Lumpkin et al*., 2002; *Zhurbas and Oh*, 2003]. This apparent conflict can be resolved by noting that those earlier studies included all drifter trajectories, both from loopers and nonloopers. For nonloopers, the integral time scale can be calculated by integrating the autocorrelation function to the first zero crossing, assuming that values after this are dominated by noise [*Lumpkin et al*., 2002]; for the drifters in the subtropical North Atlantic region of Figure 8, this yields an integral time scale of ~1.5 days—considerably shorter than the 8.6 day median value of T_L for the loopers in the region. Because 8% of the observations in the region are loopers, this suggests that the overall mean T_L is ~2 days, close to the ~3 day value found by *Lumpkin et al*. [2002] in this region.

Figure 9 shows the globally averaged velocity spectra of loopers and nonloopers. The spectra were calculated from the detrended velocities during the first 60 days of all drogued looper or nonlooper trajectory segments of at least 60 day duration (12,258 nonlooper segments; 587 looper segments), and are the average of the zonal and meridional spectra. Also shown in Figure 9 is a Matérn process of the form $E(f) = B^2/(f^2 + h^2)^\delta$ [*Sykulski et al*., 2013], with $B = 0.011$ m^2/s^2, $h = 0.1$ cpd, and $\delta = 1.6$ to match the globally averaged nonlooper spectrum. The parameter δ determines the power law spectral slope at large f (where the slope is -2δ) and thus the nature of the turbulent motion: $\delta = 1$ corresponds to standard Brownian motion, while fractional stochastic processes have noninteger δ [cf. *Sykulski et al*., 2013]. The value found here is close to $\delta = 1.65$ found by *Rupolo et al*. [1996]. Rupolo et al. noted that Lagrangian spectra can be generally characterized by a low-frequency plateau, a high-frequency dropoff, and an intermediate regime, and concluded that "[t]he existence of an intermediate power law

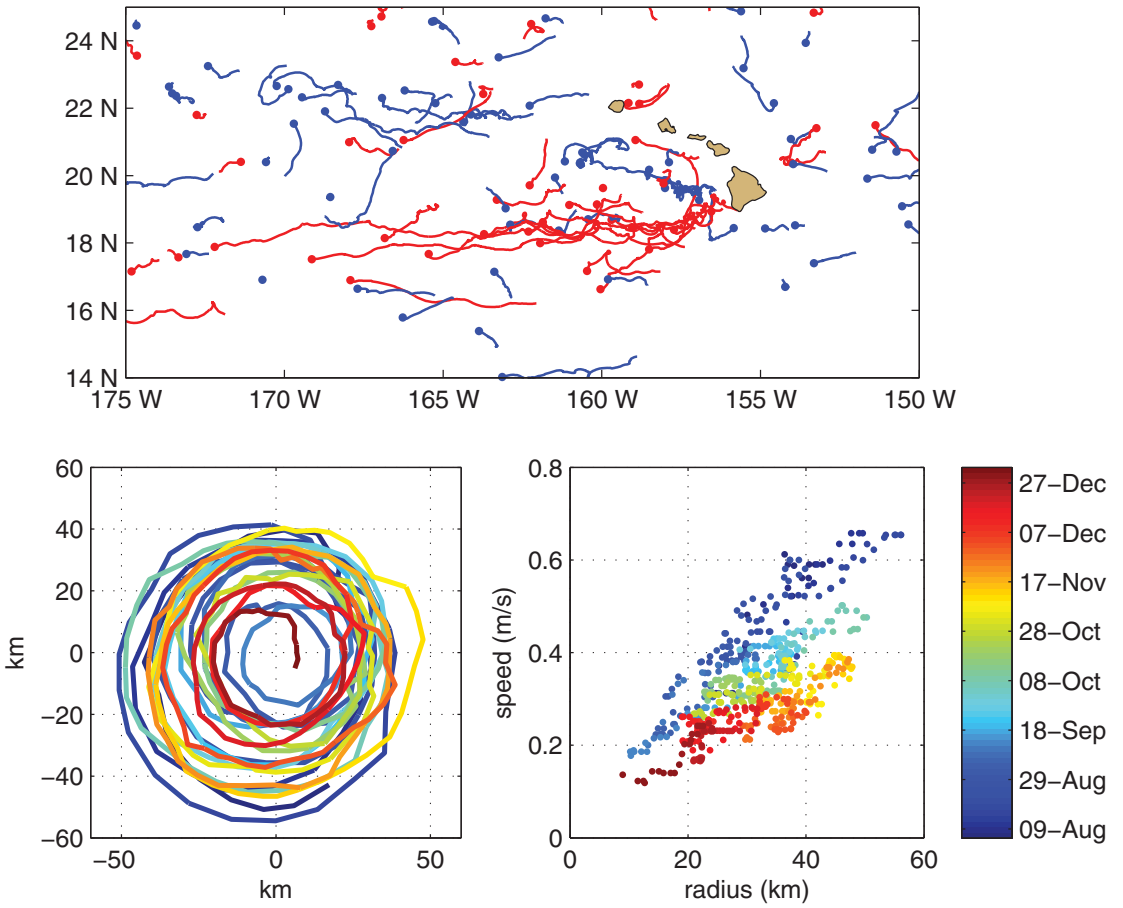

Figure 7. (top) pathways of cyclonic (blue) and anticyclonic (red) vortices derived from looper trajectory segments. Dots indicate the final location of the vortex center. (bottom left) Trajectory of drifter 22938, caught in a long-lived anticyclone that propagated from the Big Island to 172°W, in frame of reference of vortex center. Colors indicate date in 2003. (bottom right) Velocity in moving frame of reference as function of distance from vortex center.

behavior in the spectrum can be linked with the trapping of some trajectories by persistent energetic structures and is associated with a tendency for anomalous diffusion lasting up to $10T_L$." This conclusion is consistent with the enhanced lobe of energy found in the looper spectrum at ~0.04–0.3 cpd that is entirely missing from the nonlooper spectrum, which transitions smoothly from the low-frequency plateau to the high-frequency dropoff.

Figure 10 (top) shows the time-mean total kinetic energy (TKE) of all drogued nonloopers and loopers in the Gulf Stream region, calculated by simple bin averaging. The TKE along the time-averaged path of the Gulf Stream is dominated by the mean kinetic energy found in nonlooper trajectories, which exceeds 0.7 m^2/s^2 in some bins. Off the Gulf Stream path, maximum TKE is associated with the eddy kinetic energy fluctuations found in the looper trajectories. Figure 10 (bottom) shows the time-mean speeds of nonlooper and looper trajectories. The average speed of the nonloopers reveals the classical Gulf Stream current system: the Loop Current, Florida Current, Gulf Stream, Gulf Stream Extension, and Azores Current, among other features common in time-mean surface velocity maps of the region. Maximum Gulf Stream speeds exceed 1.2 m/s. However, the mean speeds of loopers are dramatically different: apart from a weakened Gulf Stream along the U.S. east coast and an extremely abbreviated extension, the major currents are not present in the mean looper map. The lack of a robust Gulf Stream Extension east of 40°W is not surprising when the mean displacement of eddies in the region is examined: the Gulf Stream rings which have trapped looper trajectories in this region propagate westward, north or south of the instantaneous Gulf Stream path, and thus a weak westward current exists in the time-mean looper map in place of the eastward Gulf Stream Extension. It is for this reason that the time-mean currents were not removed prior to identifying loopers, as their time-mean currents are significant different from those of nonloopers. The time-mean currents only appear in the mean looper velocity map in places where drifter-trapping vortices are advected by a relatively stationary time-mean flow. Maps

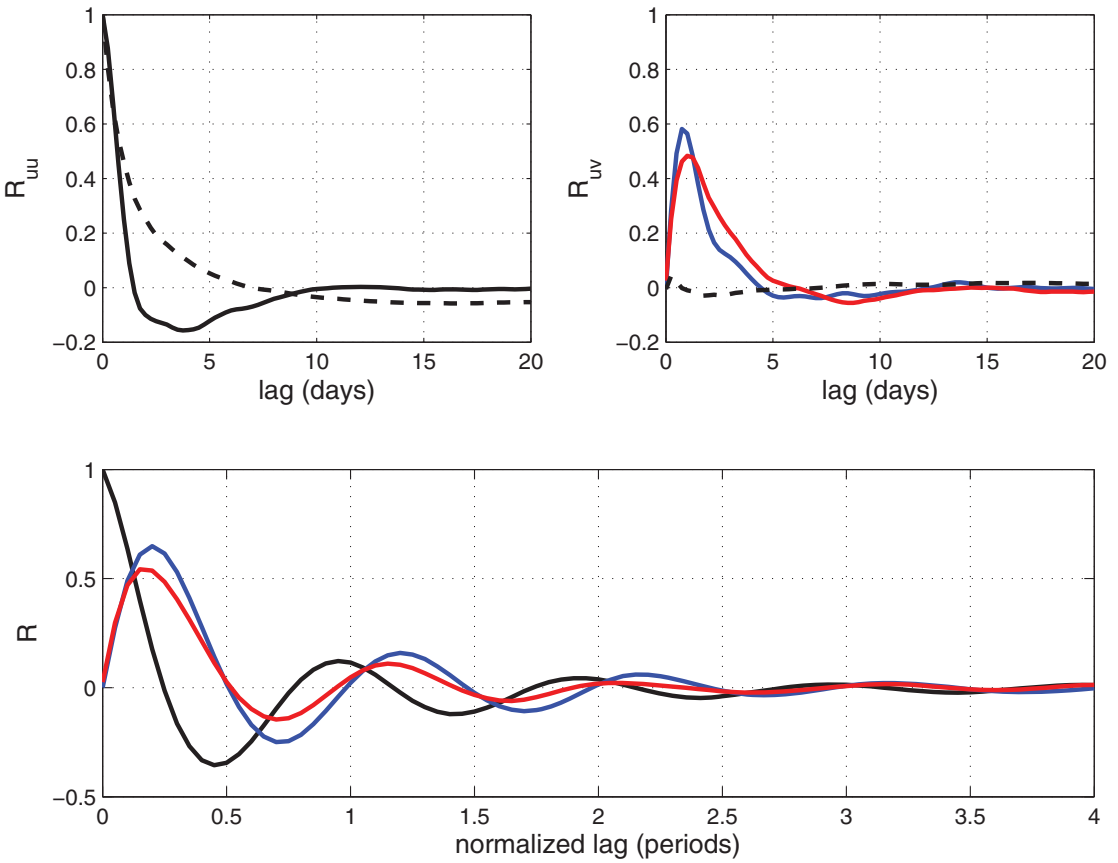

Figure 8. Mean auto-correlation and cross-correlation functions for drifter trajectory segments in the subtopical North Atlantic region 18°N–32°N, 30°W–72.5°W (cf., Figure 1 of GLV08). (top left) Autocorrelation of loopers (solid) and nonloopers (black). (top right) Cross correlation of anticyclonic loopers (red), nonloopers (black), and −1 times the cross correlation of cyclonic loopers (blue). (bottom) Auto (black) and cross correlation (red, blue) of loopers, as in top plot, but with lag normalized by period for each segment before averaging.

of time-mean spin Ω (Figure 10, bottom), which is proportional to time-mean vorticity in the presence of solid-body rotation [*Veneziani et al.*, 2005], are dominated by looper trajectory segments.

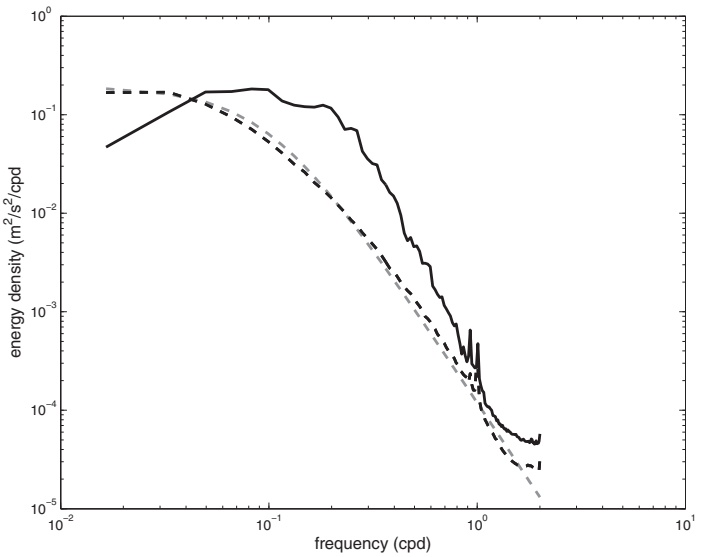

Figure 9. Globally averaged velocity spectra of loopers (solid) and nonloopers (dashed black), and fit to nonlooper spectrum (dashed grey).

Globally, the difference between looper and nonlooper mean zonal velocity is shown in Figure 11. Loopers exhibit significant westward anomalies (negative values in Figure 11) in the time-mean locations of the Gulf Stream, Kuroshio, Agulhas Retroflection, and Antarctic Circumpolar currents, all eastward-flowing currents in the time-mean nonlooper velocities. Loopers trapped within Tropical Instability Waves move dramatically faster to the west than nonloopers in this latitude band. In the low-latitude bands dominated by submesoscale cyclonic vortices, the loopers move less quickly to the west than the time-mean currents, producing eastward anomalies in

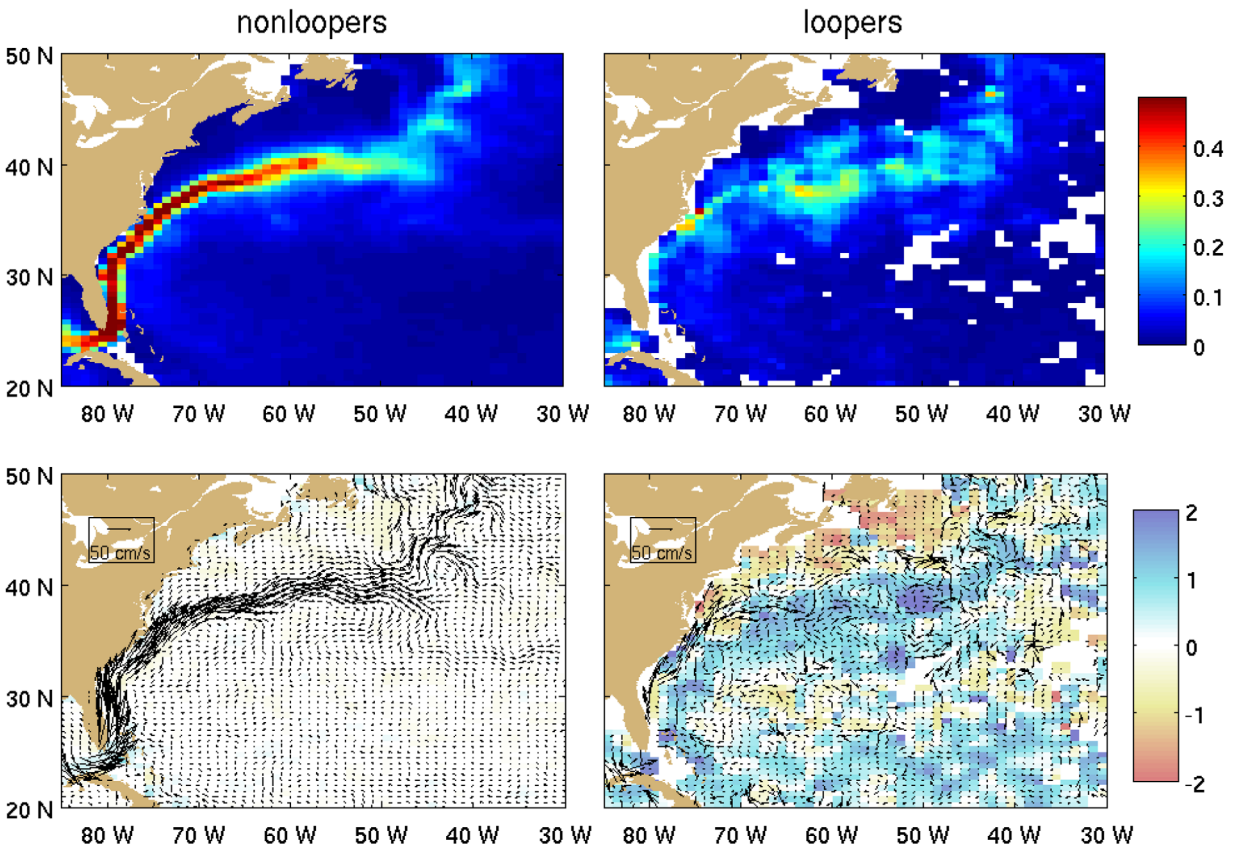

Figure 10. (top) Time-mean total kinetic energy (shading; m^2/s^2) of (left) drogued nonloopers and (right) loopers in the Gulf Stream region. (bottom) Time-mean spin Ω (shading; 10^{-5} s^{-1}), and velocity (arrows) of (left) nonloopers and (right) loopers. Both plots use the same color range for spin.

those bands. This is not primarily due to seasonal sampling biases, although most loopers in this region are seen in Austral winter and spring (consistent with the known seasonality of submesoscale variability [*Callies et al.*, 2015]) when the currents can be weaker. For example, in the South Equatorial Current band 0°W–30°W, 10°S–20°S, the monthly averaged zonal speed of both loopers and nonloopers show similar seasonal variations with peak westward speeds in January [e.g., *Lumpkin and Garzoli*, 2005], with an approximately constant offset of 7–8 cm/s (nonloopers faster). The slower propagation speed of vortices compared to larger-scale variations, particularly in the band 20°S–20°N, is discussed in *Chelton et al.* [2011].

5. Discussion

There is a considerable body of work examining propagating features in altimetry [e.g., *Chelton et al.*, 2007, 2011, and references therein]. Although initially interpreted as Rossby waves, subsequent analysis of the geometry and nonlinearity of these features concluded that they were predominantly coherent vortices which could transport water for long distances [*Chelton et al.*, 2007]. This is unquestionably the case for the loopers tracked in this study, which in many cases indicate that the drifters were transported over large distances. The eddy census data of *Chelton et al.* [2011], updated through April 2012, can be compared to the vortex center locations determined from the loopers. This altimetry-derived data set includes eddy center location at 7 day increments, as well as the eddy amplitude, radius, and sign of vorticity (cyclonic or anticyclonic), at 7 day increments during the period October 1992 to April 2012. For comparison to this, the drifter-derived vortex center locations are decimated to the same 7 day values for this time period. For each 7 day location, the nearest concurrent altimeter-derived eddy center is identified; if the distance is less than D_{thresh} and the sign (cyclonic or anticyclonic) is the same, the location is considered to be a match (i.e., present in both data sets). A range of values for D_{thresh} was considered: the fraction of matches increases with increasing D_{thresh}, with 42% of the drifter-derived eddy centers matching altimeter-derived centers for

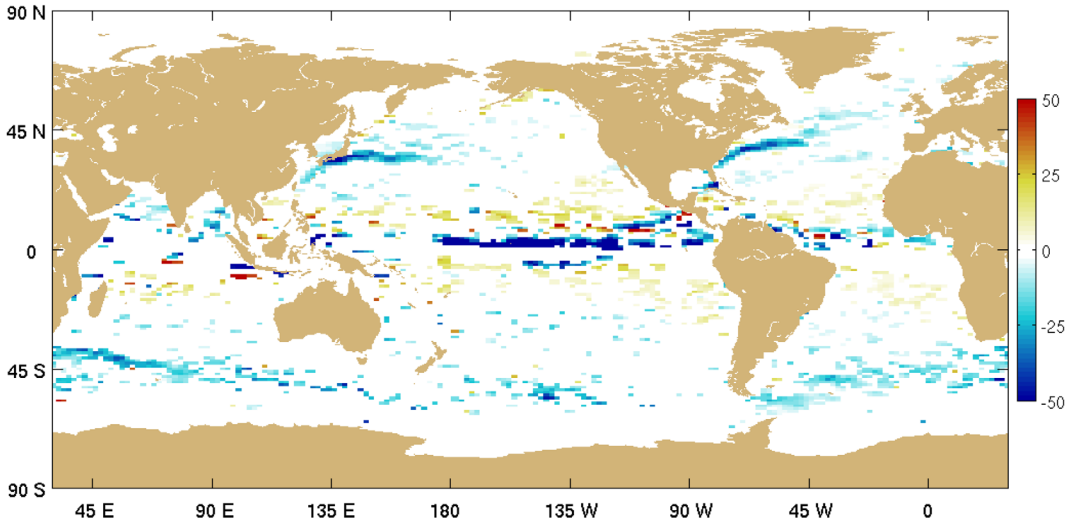

Figure 11. Time-mean eastward velocity of loopers minus nonloopers (cm/s), shown only where results are significantly different from zero by at least one standard error.

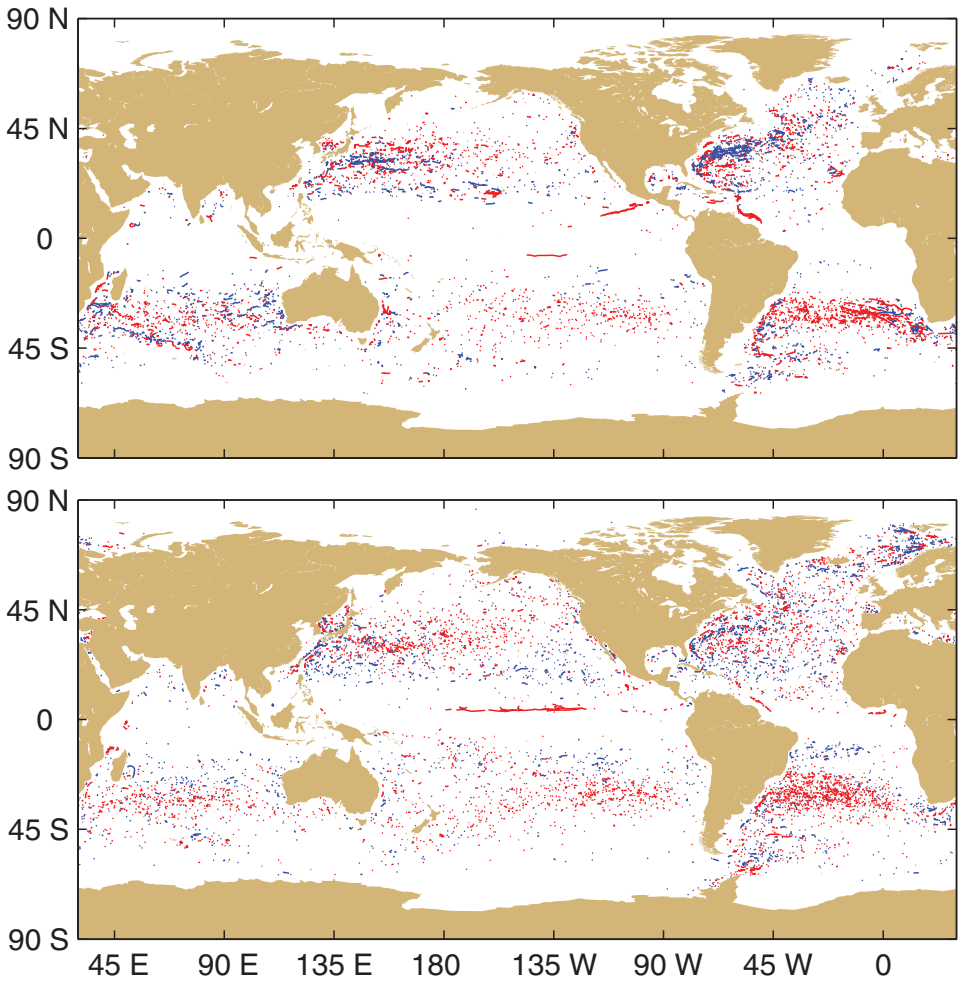

Figure 12. Seven day locations of cyclonic (blue) and anticyclonic (red) vortex centers derived from looping drifter trajectory segments which (top) match or (bottom) do not match eddy center locations determined from altimetry [*Chelton et al.*, 2011]. The altimeter data span the period October 1992 to April 2013.

D_{thresh} =1°, 59% matching for D_{thresh} = 2°, and 66% matching for D_{thresh} = 3°. The median spacing of vortices in the altimeter-derived data set is 2.1° and the vortices fill most of the worlds' oceans (albeit less densely at low latitudes), suggesting that values much greater than D_{thresh} = 2° will result in a ~50% chance of a spurious match (assuming a 50/50 distribution of vorticity). This likely accounts for the plateau in matches for D_{thresh} > 2°. Matches and nonmatches are shown in Figure 12 for D_{thresh} = 1°. The median looper radius of the matches is 30 km while the median looper radius of nonmatches is 17 km, indicating that one major reason some loopers are not found in the altimeter-derived data is that they are orbiting a vortex too small to be resolved in altimetry. Supporting this hypothesis, 27% of the nonmatches had looping radii less than 10 km compared to only 9% of the matches. It is clear from Figure 12 that the majority of the cyclonic submesoscale vortices at ~20°N/S are not found in the altimeter-derived eddy census. In addition, it is interesting to note that a relatively small fraction of the eddy features seen in altimetry are *not* associated with coherent vortices trapping looping drifters: nonloopers were found within 1° of an altimeter-derived eddy in only 2705 of the 6565 eddies in the altimeter data set, while loopers were found in 3039 of them. As noted earlier, only 7.6% of the drifter observations were made by loopers, so one would expect many more nonloopers matches with altimeter-derived eddies if they were not generally associated with vortices fluid trapping. This result is not consistent with *Beron-Vera et al*. [2013], who concluded that many of the features in the *Chelton et al*. [2011] data set are not coherent vortices.

In this study, looper drifter trajectory segments were automatically identified by an algorithm developed as an extension of GLV08. By applying this algorithm to Global Drifter Program data going back to 1979, over 15,000 looping trajectory segments were identified worldwide. Two-thirds of these segments persist in looping for 14–39 days, while one-third loop for less time and one-third loop longer. Some loop for hundreds of days; the longest looper in the record persisted for 287 days. The paths taken by the vortices at the center of these looper trajectory segments can be calculated automatically, allowing analyses in a frame of reference moving with the vortices.

The Lagrangian integral time scale can be estimated from the velocity autocorrelation and cross correlation of each looper segment, and is generally very close to the orbital period. Values range from ~5 days at high latitudes to ~10 days at 20°N/S, and are ~20 days in TIW-associated loopers. These values are more than twice as large as typical integral time scales for the overall drifter data set (dominated by nonloopers) at comparable latitudes [e.g., *Zhurbas and Oh*, 2003, Figure 6], a fascinating result. The integral time scale characterizes diffusive motion in the ocean; clearly, values within coherent vortices are dramatically different than those in the turbulent sea surrounding them. This result is consistent with coherent vortices acting as transport barriers and trapping, at least for a while, the drifters within them.

Time-mean quantities such as total kinetic energy and speed can be significantly different between looper and nonlooper trajectory segments. For some purposes, such as creating maps of time-mean velocity, the looper data may be considered as (very energetic) noise which could be eliminated prior to calculating means. A more careful approach to the data might require separately calculating means of the nonloopers and loopers, and only afterward combining the results for an overall time-mean picture.

Acknowledgments

This paper was funded by the Atlantic Oceanographic and Meteorological Laboratory and the Climate Observation Division, Climate Program Office, both of the National Oceanic and Atmospheric Administration, U.S. Department of Commerce. The 6 hourly observations comprising drifter trajectory segments identified in this study as loopers are available at http://www.aoml.noaa.gov/phod/loopers/. Conversations and suggestions from Renellys Perez, Jonathan Lilly, Josefina Olascoaga, Javier Beron-Vera, Chris Meinen, Amy Bower, Annalisa Griffa, and two anonymous reviewers were extremely valuable. The drifter data were collected and are made freely available by NOAA's Global Drifter Program at http://www.aoml.noaa.gov/envids/gld/index.php. The altimeter-derived eddy census of *Chelton et al*. [2011], updated through April 2012, is available at http://cioss.coas.oregonstate.edu/eddies/.

References

Beron-Vera, F. J., Y. Wang, M. J. Olascoaga, G. J. Goni, and G. Haller (2013), Objective detection of oceanic eddies and the Agulhas leakage, *J. Phys. Oceanogr.*, *43*, 1426–1438, doi:10.1175/JPO-D-12-0171.1.

Callies, J., R. Ferrari, J. M. Klymak, and J. Gula (2015), Seasonality in submesoscale turbulence, *Nat. Commun.*, *6*, 6862, doi:10.1038/ncomms7862.

Chelton, D. B., M. G. Schlax, R. M. Samelson, and R. A. de Szoeke (2007), Global observations of large oceanic eddies, *Geophys. Res. Lett.*, *34*, L15606, doi:10.1029/2007GL030812.

Chelton, D. B., M. G. Schlax, and R. M. Samelson (2011), Global observations of nonlinear mesoscale eddies, *Prog. Oceanogr.*, *91*(2), 167–216, doi:10.1016/j.pocean.2011.01.002.

Dong, C., Y. Liu, R. Lumpkin, M. Lankhorst, D. Chen, J. McWilliams, and Y. Guan (2011), A scheme to identify loops from trajectories of oceanic surface drifters: Application to the Kuroshio extension region, *J. Atmos. Oceanic Technol.*, *28*, 1167–1176, doi:10.1175/JTECH-D-10-05028.1.

Elipot, S. K. Y. (2006), Spectral characterization of Ekman velocities in the Southern Ocean based on surface trajectories, PhD dissertation, Scripps Inst. of Oceanogr., Univ. of Calif., San Diego. [Available at http://repositories.cdlib.org/sio/techreport/49/.]

Flament, P., R. Lumpkin, J. Tournadre, and L. Armi (2001), Vortex pairing in an unstable anticyclonic shear flow: Discrete subharmonics of one pendulum day, *J. Fluid Mech.*, *440*, 401–409, doi:10.1017/S0022112001004955.

Flierl, G. R. (1981), Particle motions in large-amplitude wave fields, *Geophys. Astrophys. Fluid Dyn.*, *18*, 39–74.

Griffa, A., R. Lumpkin, and M. Veneziani (2008), Cyclonic and anticyclonic motion in the upper ocean, *Geophys. Res. Lett.*, *35*, L01608, doi:10.1029/2007GL032100.

Hansen, D., and P.-M. Poulain (1996), Quality control and interpolations of WOCE-TOGA drifter data, *J. Atmos. Oceanic Technol.*, *13*, 900–909, doi:10.1175/1520-0426(1996)013 < 0900:QCAIOW>2.0.CO;2.

Lilly, J. M., and S. C. Olhede (2010), Bivariate instantaneous frequency and bandwidth, *IEEE Trans. Signal Process.*, *58*, 591–603.
Lilly, J. M., R. K. Scott, and S. C. Olhede (2011), Extracting waves and vortices from Lagrangian trajectories, *Geophys. Res. Lett.*, *38*, L23605, doi:10.1029/2011GL049727.
Lumpkin, R., and P. Flament (2001), Lagrangian statistics in the central North Pacific, *J. Mar. Syst.*, *29*, 141–155, doi:10.1016/S0924-7963(01)00014-8.
Lumpkin, R., and S. L. Garzoli (2005), Near-surface circulation in the Tropical Atlantic Ocean, *Deep Sea Res., Part I*, *52*(3), 495–518, doi:10.1016/j.dsr.2004.09.001.
Lumpkin, R., and Z. Garraffo (2005), Evaluating the decomposition of tropical Atlantic drifter observations, *J. Atmos. Ocean. Techn.*, *22*(9), 1403–1415, doi:10.1175/JTECH1793.1.
Lumpkin, R., and G. Johnson (2013), Global ocean surface velocities from drifters: Mean, variance, ENSO response, and seasonal cycle, *J. Geophys. Res. Oceans*, *118*, 2992–3006, doi:10.1002/jgrc.20210.
Lumpkin, R., and M. Pazos (2007), Measuring surface currents with Surface Velocity Program drifters: The instrument, its data and some recent results, in *Lagrangian Analysis and Prediction of Coastal and Ocean Dynamics*, edited by A. Griffa et al., chap. 2, pp. 39–67, Cambridge Univ. Press, Cambridge, U. K.
Lumpkin, R., A.-M. Treguier, and K. Speer (2002), Lagrangian eddy scales in the northern Atlantic Ocean, *J. Phys. Oceanogr.*, *32*, 2425–2440, doi:10.1175/1520-0485-32.9.2425.
Lumpkin, R., S. Grodsky, L. Centurioni, M.-H. Rio, J. Carton, and D. Lee (2012), Removing spurious low-frequency variability in drifter velocities, *J. Atmos. Oceanic Technol.*, *30*(2), 353–360, doi:10.1175/JTECH-D-12-00139.1.
Lumpkin, R., and Z. Garraffo (2005), Evaluating the decomposition of tropical Atlantic drifter observations, *J. Atmos. Ocean. Techn.*, *22*(9), 1403–1415, doi:10.1175/JTECH1793.1.
Niiler, P. P., A. Sybrandy, K. Bi, P. Poulain, and D. Bitterman (1995), Measurements of the water-following capability of holey-sock and TRISTAR drifters, *Deep Sea Res., Part I*, *42*, 1951–1964, doi:10.1016/0967-0637(95)00076-3.
Richardson, P. L. (1993), A census of eddies observed in North Atlantic SOFAR float data, *Prog. Oceanogr.*, *31*, 1–50, doi:10.1016/0079-6611(93)90022-6.
Rupolo, V., V. Artale, B. L. Hua, and A. Provenzale (1996), Lagrangian velocity spectra at 700 m in the Western North Atlantic, *J. Phys. Oceanogr.*, *26*, 1591–1607, doi:10.1175/1520-0485(1996)026 <1591:LVSAMI>2.0.CO;2.
Stammer, D. (1997), Global characteristics of ocean variability estimated from regional TOPEX/POSEIDON altimeter measurements, *J. Phys. Oceanogr.*, *27*, 1743–1769, doi:10.1175/1520-0485(1997)027 <1743:GCOOVE>2.0.CO;2.
Sykulski, A. M., S. C. Olhede, J. M. Lilly, and E. Danioux (2013), Lagrangian time series models for ocean surface drifter trajectories, *Stat. Sci. Res. Rep. 322*, Cornell Univ., Ithaca, N. Y.
Veneziani, M., A. Griffa, A. M. Reynolds, and A. J. Mariano (2004), Oceanic turbulence and stochastic models from subsurface Lagrangian data for the Northwest Atlantic Ocean, *J. Phys. Oceanogr.*, *34*, 1884–1906, doi:10.1175/1520-0485(2004)034 <1884:OTASMF>2.0.CO;2.
Veneziani, M., A. Griffa, Z. D. Garraffo, and E. P. Chassignet (2005), Lagrangian spin parameter and coherent structures from trajectories released in a high-resolution ocean model, *J. Mar. Res.*, *63*, 753–788.
Veneziani, M., A. Griffa, Z. Garraffo, and J. A. Mensa (2014), Barrier layers in the tropical South Atlantic: Mean dynamics and submesoscale effects, *J. Phys. Oceanogr.*, *44*, 265–288, doi:10.1175/JPO-D-13-064.1.
Zhurbas, V. M., and I. S. Oh (2003), Lateral diffusivity and Lagrangian scales in the Pacific Ocean as derived from drifter data, *J. Geophys. Res.*, *108*(C5), 3141, doi:10.1029/2002JC001596.